The 7th Iranian Aerospace Society Conference
Feb. 19-21/2008, Sharif University of Technology

IAS-2008-PR0570

Numerical Simulation of Partial Cavitation over Axisymmetric Bodies: VOF Method vs. Potential Flow Theory

Mohammad P. Fard[1], H. Moin[2], I. Rashidi[3] and Mahmoud P. Fard[4]
Department of Mechanical Engineering, Ferdowsi University of Mashhad, Mashhad, Iran

Abstract

A computational study of partial cavitation over axisymmetric bodies is presented using two numerical methods. The first method is based on the VOF technique where transient Navier-Stokes equations are solved along with an equation to track the cavity interface. Next, the steady boundary element method (BEM) based on potential flow theory is presented. The results of the two methods for a disk cavitator are compared with each other and with those of the available experiments and analytical relations. The two methods are then used to predict the partial cavity over an axisymmetric body consisting of a disk cavitator followed by a conical section and ending in a cylindrical shape. The effects of various parameters such as cone length, cone angle, cavitator radius and cylinder diameter are investigated. Shortcomings and limitations of each method are discussed.

Keywords: *"cavitation", "VOF method", "boundary element Method"*

Introduction

The cavitation phenomenon is known as liquid vaporization that occurs whenever the liquid pressure falls bellow its vapor pressure. This phenomenon is categorized by a nondimensional parameter called cavitation number defined as:

$$\sigma = \frac{P_\infty - P_v}{\frac{1}{2}\rho V_\infty^2} \qquad (1)$$

where P_v is the vapor pressure, ρ the liquid density, and P_∞, V_∞ are the ambient pressure and inflow velocity, respectively. The cavitation regimes are classified to incipient-, shear-, cloud-, partial- and super-cavitation depending on the cavitation number [1]. The cavitation occurs around axisymmetric bodies at points where the local pressure drops to the environment vapor pressure. Any sudden change in the body shape may cause a pressure rise or fall and, therefore, may be an inception point for cavitation. Although super-cavitation decreases drag forces extensively, but when maneuvering of the vehicle is necessary, partial cavitation is more preferable [2]. Also, partial cavities are widely used in ventilated systems [2, 3].

During the last decades, numerous studies have been performed in cavitation using various methods [1]. Cavitation models based on the Navier-Stokes equations emerged in early 1990's. These models are divided into two main categories: interface tracking method and homogeneous equilibrium flow [1, 4]. In interface tracking method, a constant pressure (vapor pressure) is assumed for the cavity region and a wake model is used to predict the shape of the cavity in adaptive grids. In the second category, used in this study, the density field is estimated by various models from which the method based on single-fluid modeling has been shown to be more accurate [1]. In this approach, an advection equation for liquid (or vapor) volume fraction is solved and the density is computed according to the volume fraction of the two phases. This approach has been widely applied to simulate cavitation. The selection of an appropriate mass transfer model and an algorithm for advection equation are the main issues. Yuan et al. [5] suggested a cavitation model based on Rayleigh relation. Singhal et al. [6], Merkle et al. [7] and Kunz et al. [8] have used different mass transfer models based on semi-analytical equations. A well-known method to solve the advection of a free-surface such as a cavity interface is VOF technique. Frobenius and Schilling [9] and Wiesche [10] used this technique to simulate cavitation over hydrofoils and pump impellers. A review of the reported literature reveals that VOF method can accurately capture cavity shape and characteristics. In this study, a modified VOF technique based on Youngs' PLIC algorithm [11] is combined with a mass transfer model of Kunz et al. [8] to simulate cavitation.

A different type of model used by many researchers for studying cavitation is Boundary Element Method (BEM). Early researches based on this technique in partial-cavitation flows were performed by Varghese, et al. [2], but using BEM to solve potential flow about arbitrary bodies were developed after Hess and Smith's paper [12]. Nonlinear BEM method were developed for cavitating flows around hydrofoils by Uhlman [13, 14], and Kinnas and Fine [15, 16]. They distributed sources and normal dipoles along the solid body-cavity interface. The unknown values of these sources and dipoles were determined by imposing the dynamic condition on an assumed cavity boundary. The kinematic boundary condition was then used to update the cavity shape. Beginning in 1994, two numerical hydrodynamics models were developed for axisymmetric supercavitating high-speed bodies: a

[1]Assistant professor and corresponding author (mpfard@um.ac.ir)
[2]M.Sc. student
[3]PhD candidate
[4]Assistant professor

slender-body theory model (Varghese, et al, [17]) and a BEM method (Kirschner, et al, [18]; Uhlman, et al, [19]). The results of both the slender-body theory and the BEM method have been shown to compare well with other numerical and experimental results. These models can predict the shape and length of cavity, accurately. The BEM method was employed to examine supercavitating flows past disk, cone and sigma-shaped cavitators where good agreement with experimental and analytical results have been reported [20].

In this paper, partial cavitation for water flows over axisymmetric bodies is studied using two general types of models mentioned above. For the VOF method, a modified Youngs' PLIC algorithm is used to advect the interface between the two phases (cavity). For the BEM method, sources and normal dipoles are distributed along the body-cavity surface. The unknown values of the source and dipole strengths are then obtained using the mixed Fredholm integral equation that results from the application of Green's third identity.

Governing Equations

The two methods of VOF and BEM are briefly discussed in this section. The VOF method is based on the solution of the full Navier-Stokes equations along with an equation for the advection of cavity interface. The BEM method, however, is based on the concept of potential flow theory.

1. Volume-of-Fluid Method (VOF)

In this method, the advection of the cavity interface is simulated based on the Volume-of-Fluid (VOF) technique along with a cavitation model for mass transfer between the two phases of liquid and vapor.

1.1. VOF Algorithm

The governing equations for the 2D/axisymmetic incompressible fluid flow are

$$\vec{\nabla}.\vec{V} = 0 \tag{2}$$

$$\frac{\partial \vec{V}}{\partial t} + \vec{\nabla}.(\vec{V}\vec{V}) = -\frac{1}{\rho}\vec{\nabla}P + \frac{1}{\rho}\vec{\nabla}.\vec{\tau} + \frac{1}{\rho}\vec{F}_b + \vec{g} \tag{3}$$

where $\vec{V}$ is the velocity vector, P indicates the pressure, F_b is body force acting on fluid, $\vec{g}$ is the acceleration due to gravity and τ represents Newtonian viscous stress tensor. In VOF method, the phase change boundary is simulated by a scalar field f whose value is equal to zero in the vapor phase and one in the liquid. When a cell is partially filled with liquid, f has a value between zero and one. The discontinuity in f is propagating through the computational domain according to:

$$\frac{df}{dt} = \frac{\partial f}{\partial t} + \vec{V}.\vec{\nabla}f = S \tag{4}$$

where S is the cavitation mass transfer sink term. This equation with different mass transfer models can be used to simulate many physical phenomena such as cavitation, vaporization, and condensation. The Hirt-Nichols [21] and Young PLIC [11] methods are widely used for the advection of the volume fraction f in Eq. 4. Although the Hirt-Nichols has been used in most cavity simulations, in this study a more accurate method of Young is employed. To begin the advection using Eq. 4, an intermediate value of f is introduced as:

$$\tilde{f} = f^n - \delta t\,\vec{\nabla}.(\vec{V}f^n) \tag{5}$$

and "divergence correction" completes the scheme:

$$f^{n+1} = \tilde{f} + \delta t(\vec{\nabla}.\vec{V})f^n + \delta t(S^n) \tag{6}$$

This scheme initiates the distribution of f for velocity and pressure calculations in each time step. Because a single set of equations is solved for both phases, mixture properties are used as:

$$\begin{aligned} \rho &= f\rho_l + (1-f)\rho_v \\ \mu &= f\mu_l + (1-f)\mu_v \end{aligned} \tag{7}$$

where subscripts l and v denote the liquid and vapor, respectively. Two-step time projection method is employed for the solution of momentum equations. First an intermediate velocity is calculated based on the terms related to advection, viscosity and body forces:

$$\frac{\tilde{\vec{V}} - \vec{V}^n}{\delta t} = -\vec{\nabla}(\vec{V}\vec{V})^n + \frac{1}{\rho^n}\vec{\nabla}.\vec{\tau} + \vec{g}^n + \frac{1}{\rho^n}\vec{F}_b^n \tag{8}$$

Continuum Surface Force (CSF) method [22] is used to treat the surface tension in interfacial cells as a body force. Pressure field is obtained by Poisson equation as:

$$\vec{\nabla}.(\frac{1}{\rho}\vec{\nabla}P^{n+1}) = \frac{\vec{\nabla}.\tilde{\vec{V}}}{\delta t} \tag{9}$$

Finally, the pressure field is used to compute the new time velocities:

$$\frac{\vec{V}^{n+1} - \tilde{\vec{V}}}{\delta t} = -\frac{1}{\rho}\vec{\nabla}P^{n+1} \tag{10}$$

An Incomplete Cholesky Conjugate Gradient Decomposition (ICCG) solver is employed for solving Eq. 9. Having calculated the new time level pressures, the velocities are updated using Eq. 9.

1.2. Cavitation Model

Several cavitation mass transfer models can be used to replace S in Eq. 4. Among the more recommended models we have the Rayleigh equation and semi-analytical schemes [1]. Many semi-analytical schemes are based on the modified Rayleigh theory or a mass-momentum interaction model around the cavity interface [23]. In current study, the semi-analytical model of Kunz is used to treat S in Eq. 4:

$$\begin{aligned} \frac{\partial f}{\partial t} + \vec{V}.\vec{\nabla}f = {} & \frac{C_{dest}\rho_l Min(P_l - P_v, 0)f}{(\tfrac{1}{2}\rho_l V_\infty^2)\rho_v t_\infty} \\ & + \frac{C_{prod}(1-f)f^2}{\rho_l t_\infty} \end{aligned} \tag{11}$$

where $C_{dest} = 9\times10^5$ and $C_{prod} = 3\times10^4$ are numerical-experimental weighting coefficients. The flow characteristic time, t_∞, is defined as the ratio of the maximum solid-body diameter to the main flow velocity. The second term in the right hand side of Eq. 11 is for the condensation that occurs near the cavity closure region. This phenomenon causes small vapor

structures to detach from the end of the cavity. The Kunz model assumes a moderate rate of constant condensation; therefore, it reconstructs the cavity region more accurately than the other models [1, 23].

2. Boundary Element Method (BEM)

This section explains the BEM cavitation model based on the potential flow theory.

2.1 Mathematical Formulation

The potential flow model presented here is based on Green's third identity formulation [15]. Applying this formulation to the axisymmetric disturbance velocity potential, φ, results in:

$$2\pi\varphi(r,x) = \iint_S \left\{ \frac{\partial\varphi}{\partial n} G(x,r;\xi,R) - \varphi(r,x)\frac{\partial G(x,r;\xi,R)}{\partial n} \right\} R\,d\varphi\,ds \tag{11}$$

where n is the normal vector directed outward from the solid-body surface and the cavity interface, s is the arclength along a meridian, and x and r are the components of the axisymmetric coordinate system. $G(x,r;\xi,R)$ is the potential function related to the fluid sources distributed along a ring of radius R located on the axis at $x=\zeta$ (see Fig 1). The potential function is defined as:

$$G(x,r;\xi,R) = \int_{-\pi}^{+\pi} \frac{\rho\, d\varphi}{\sqrt{(x-\xi)^2 + r^2 + R^2 - 2rR\cos(\varphi)}} = R\mathrm{J}_1^0(A,B) \tag{12}$$

where

$$A = \mathrm{r}^2 + R^2 + (x-\xi)^2 \qquad B = 2\mathrm{r}R \tag{13}$$

and

$$\mathrm{J}_1^0(A,B) = \frac{4}{\sqrt{A+B}}\mathrm{K}(k) \qquad \mathrm{K}(k) = \int_0^{\pi/2} \frac{d\varphi}{\sqrt{1-k^2\sin^2(\varphi)}} \qquad k^2 = \frac{2B}{A+B} \tag{14}$$

The total and disturbance potentials are related by:

$$\phi = x + \varphi \tag{15}$$

where all quantities have been made dimensionless with respect to ρ, U_∞ and d . The boundary conditions are kinematic condition on the solid-body surface, and both the kinematic and dynamic conditions on the cavity interface. These conditions are mathematically formulated as:

$$\frac{\partial\phi}{\partial n} = 0 \quad \text{on } S_b \cup S_c \tag{16}$$

$$\frac{\partial\phi}{\partial s} = \sqrt{1+\sigma} \quad \text{on } S_c \tag{17}$$

where S_b and S_c are the areas of the solid-body surface and the cavity interface, respectively. These boundary conditions are equal to:

$$\frac{\partial\varphi}{\partial n} = -x_n \quad \text{on } S_b \cup S_c \tag{18}$$

and

$$\frac{\partial\varphi}{\partial s} = \sqrt{1+\sigma} - x_s \quad \text{on } S_c \tag{19}$$

where **n** and **s** are unit vectors normal and tangent to the solid-body/cavity boundary, respectively. The last boundary condition may be integrated to yield

$$\varphi = \varphi_0 + \sqrt{1+\sigma}(s-s_0) - (x-x_0) \text{ on } S_c \tag{20}$$

where φ_0 , is the potential at the detachment point of the cavity on the solid body.

2.2 Governing Integral Equation

Placing the unknowns on the left-hand side and the knowns on the right-hand side, Green's third identity is written as:

$$2\pi\varphi + \iint_{S_b}\varphi\frac{\partial G}{\partial n}dS - \iint_{S_c}\frac{\partial\varphi}{\partial n}GdS = \iint_{S_b}\frac{\partial\varphi}{\partial n}GdS - \iint_{S_c}\varphi\frac{\partial G}{\partial n}dS \tag{21}$$

on the wetted portion of the solid-body/cavity boundary and on the cavity interface:

$$\iint_{S_b}\varphi\frac{\partial G}{\partial n}dS - \iint_{S_c}\frac{\partial\varphi}{\partial n}GdS = \iint_{S_b}\frac{\partial\varphi}{\partial n}GdS - 2\pi\varphi - \iint_{S_c}\varphi\frac{\partial G}{\partial n}dS \tag{22}$$

Implementing the above boundary conditions Eq. (21) can be written as:

$$2\pi\varphi + \iint_{S_b}\varphi\frac{\partial G}{\partial n}dS - \iint_{S_c}\frac{\partial\varphi}{\partial n}GdS + \varphi_0\iint_{S_c}\frac{\partial G}{\partial n}dS + \sqrt{1+\sigma}\left[\iint_{S_c}(s-s_0)\frac{\partial G}{\partial n}dS\right] = -\iint_{S_b}x_n GdS + \iint_{S_c}(x-x_0)\frac{\partial G}{\partial n}dS \tag{23}$$

on the solid body and Eq. (22) becomes

$$\iint_{S_b}\varphi\frac{\partial G}{\partial n}dS - \iint_{S_c}\frac{\partial\varphi}{\partial n}GdS + \varphi_0\left[2\pi + \iint_{S_c}\frac{\partial G}{\partial n}dS\right] + \sqrt{1+\sigma}\left[2\pi(s-s_0) + \iint_{S_c}(s-s_0)\frac{\partial G}{\partial n}dS\right] = -\iint_{S_b}x_n GdS + \left[2\pi(x-x_0) + \iint_{S_c}(x-x_0)\frac{\partial G}{\partial n}dS\right] \tag{24}$$

on the cavity interface.

In addition to these equations, an auxiliary condition is required for which we impose the condition that the net source strength is equal to the flux through the jet, which may be expressed as:

$$\iint_{S_c}\frac{\partial\varphi}{\partial n}dS = \iint_{S_b}x_n dS \tag{25}$$

Results and Discussion

Two methods described above, were used to investigate various effects associated with an axisymmetric body consisting of a disk cavitator followed by a conical section and ending in a cylindrical shape (Fig. 2). The geometry parameters shown in Fig. 2 are nondimensionalized based on the cavitator diameter.

To validate the models, the results of the two methods are compared with each other and with those of the available experiments in the literature. Water properties at 25^{o}C are considered in this study.

1. Model Validation

Although cavitation is a complex two-phase phenomenon, analytical solutions of super-cavitation behind simple obstacles such as a disk or a sphere are available. Reichardt analytical relation [24] for super-cavitation behind axisymmetric cavitator is given by:

$$\frac{l_{cavity,\max}}{d_{cavity,\max}} = \frac{\sigma + 0.008}{\sigma(1.7\sigma + 0.066)} \tag{26}$$

$$\frac{d_{cavity_{\max}}}{D_{cavitator}} = \left[\frac{C_D}{\sigma(1-0.132\sigma^{0.5})}\right]^{0.5} \tag{27}$$

where $l_{cavity,max}$ and $d_{cavity,max}$ are the maximum length and diameter of the cavity, respectively, and $D_{cavitator}$ represents the maximum diameter of cavitator.

Palset and Schaffer proposed following analytical equation for the drag coefficient of a disk cavitator for cavitation numbers less than 1.5 [25]:

$$C_D = C_{D_0}(1 + \sigma + 0.028\,\sigma^2) \tag{28}$$

where C_{D_0} is equal to 0.8053.

The cavitation behind a disk cavitator for several cavitation numbers are simulated using both VOF and BEM methods. The results of the two methods are compared with each other and with those of analytical relations given by Eqs. 26, 27 and 28. Figure 3 compares the results of the two methods with those of the available experiments [1] and Reichardt relation (Eq. 27). As observed from the figure, the results of both models agree well with those of the experiments and the theory for high cavitation numbers ($\sigma > 0.15$). For lower cavitation numbers, while the VOF method predictions are in good agreement with Reichardt relation, the BEM method slightly overpredicts the experimental measurements.

The results from different methods and experiments for dimensionless cavity diameter versus cavitation number are shown in Figure 4. The VOF method gives a better prediction compared to that of Reichardt relation (the difference being less than 3.3%). The results of the BEM technique, however, is closer to those of the experiments. The comparison between the two methods, experiments, and Palset-Schaffer equation (Eq. 28) for the drag coefficient is displayed in Fig. 5. While the VOF model well predicts the experimental results, the BEM method underpredicts the measurements.

2. Partial Cavitation over an Axisymmetric Body

In this section, we study the partial cavitation over the axisymmetric body under consideration (Fig. 2). The effects of various parameters (cone length, cone angle, and cylinder diameter) on the shape of the cavity for different cavitation numbers are investigated.

The results of VOF model for a base case is shown in Fig. 6 for a cavitation number of σ = 0.0698. For this case: R_c=0.25, the cone angle is α=7.407°, and the cylinder radius is R_{cyl}= 0.9. In VOF method, the full Navier-Stokes equations are solved, therefore, all information regarding the flow are obtained. Figure 6 displays the shape of the cavity along with flow velocity and pressure distributions. The velocity magnitude is seen to be related to the phase of the flow, in the vapor phase the velocity has a smaller magnitude. The reentrant jet at the cavity closure region and the backward flow within the cavity is visible in the figure. The pressure in the vapor phase is seen to be constant and equal to that of the vapor pressure.

To investigate the effects of different geometric parameters, while one parameter is changed from that of the base case, other parameters are held constant. The results for each case are first presented using the VOF method. Then, a quantitative comparison is performed between the two methods of VOF and BEM.

2.1 Effect of Cone Length

To study the effect of cone length, the cone angle at α=7.407° and the cylinder diameter at R_{cyl}=0.9 were held constant. Then, by varying R_c (Fig. 2), different cone lengths (L_{cone}) were produced. Three different values of R_c were considered for this study. Figure 7 shows the results obtained from the VOF method for two values of R_c equal to 0.167 and 0.5. For the base case shown in Fig. 6 R_c was equal to 0.25. A comparison between Fig. 6 and the two images of Fig. 7 reveals that as the cone length is increased the cavity region covers a larger space; i.e. the cavity length and radius are increased. The case with R_c=0.5 needs extra attention because in this case, the cone length is decreased to the extent that no longer a cavitator exist in front of the body.

To see the effect of cone length more clearly, the dimensionless cavity length vs. cavitation number for different cone lengths (by varying R_c) are shown in Fig. 8 where the results of both VOF and BEM methods are displayed. No experimental or analytical results were available for this case. However, to show the difference between supercavitation behind a disk cavitator (no cylinder) and partial cavitation behind the axisymmetric body under consideration, the results of supercavitiaon behind a disk are also displayed in Fig. 8. Therefore, the VOF and BEM results in the figure should not be compared with experimental points and analytical curve shown in the figure. As seen from Fig. 8, while in the BEM method, the cone length makes no difference in the cavity shape, the VOF method predicts a smaller cavity when the cone length is decreased. As the cavity length is related to the inverse of the cavitation number, when cavitation number is increased (i.e. less

cavitation) the VOF and BEM results are nearing each other as seen in Fig. 8.

2.2 Effect of Cylinder Radius

The results of the VOF method for the shape of the cavity for four different R_{cyl} (nondimensional cylinder radius) are plotted in Fig. 9. For the case considered here, the cone angle α was 7.407°, R_c was 0.25 and $L_{cyl}+L_{cone}$ = 40 (see Fig. 2). The cylinder radius was R_{cyl}=0.5, 0.7, 0.9, 1.1. As seen from Fig. 9, the cylinder radius has no significant effect on cavity length. The cavity diameter, however, is decreased when the cylinder had a larger radius. The cavity detachment from the cylinder is also expected to occur in a cylinder with smaller radius.

The dimensionless cavitation length vs. cavitation number for two different cylinder radii is plotted in Fig. 10. The results of experiments and theory for supercavitation behind a disk cavitator with radius R_{disk} (i.e. with no cone and cylinder body) are also shown. For low cavitation numbers, discrepancies are observed between the results of the two methods (VOF and BEM). The two results, however, agree well when cavitation number increases (σ>0.2). It can be seen from both methods that when R_{cyl} is decreased, the shape of the cavity is nearing that of the supercavity behind a disk cavitator.

2.3 Effect of Cone Angle

The last effect considered is that of cone angle for a cylinder with $L_{cyl}+L_{cone}$ = 40 and L_{cone}=5 where R_c was 0.25. Three cone angles of 4°, 6.3°, and 10.75° were considered. Figure 11 displays the results of the VOF method for these cases. Reducing the cone angle increases both the length and diameter of the cavity region.

Figure 12 shows the dimensionless cavity length vs. cavitation number for two different cone angles. Similar to the previous figures, the experimental and theoretical results for supercavitation behind a disk cavitator are also plotted in the figure. As observed, the cavity length decreased when the cone angle increased in the same cavitation number. Differences between the two methods of VOF and BEM are seen at low cavitation numbers. However, when σ is greater than 0.2, the two results are nearing each other.

Conclusion

In this paper, the partial cavitation over axisymmetric bodies is studied using two numerical methods: the VOF technique based on the solution of the Navier-Stokes equations along with an equation for liquid volume fraction, and boundary element method (BEM) based on the potential flow theory. The results of the two models agree well with each other and with those of the experiments and theory for a disk cavitator. For an axisymmetric body with a front cavitator, while the two results are in good agreement for large cavitation numbers, discrepancies are seen for σ<0.2. The effect of different geometric parameters of a general shape of an axisymmetric body is also investigated using the two methods.

Figures

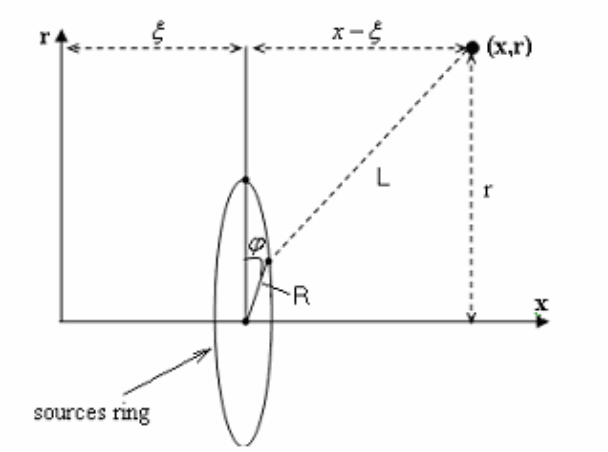

Fig. 1 Source ring in a cylindrical coordinate.

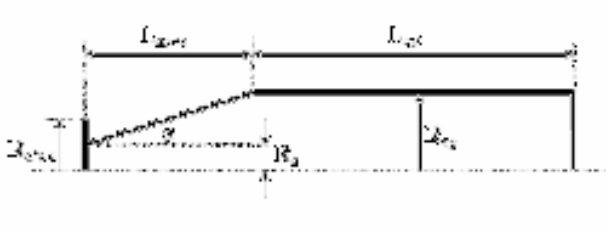

Fig. 2 Schematic of the axisymmetric body.

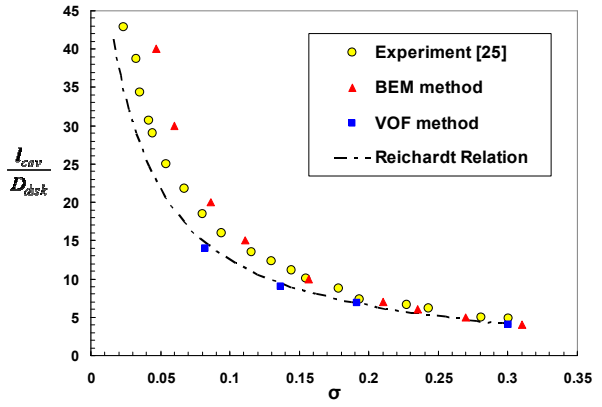

Fig. 3 Dimensionless cavity length vs. cavitation number for a disk cavitator.

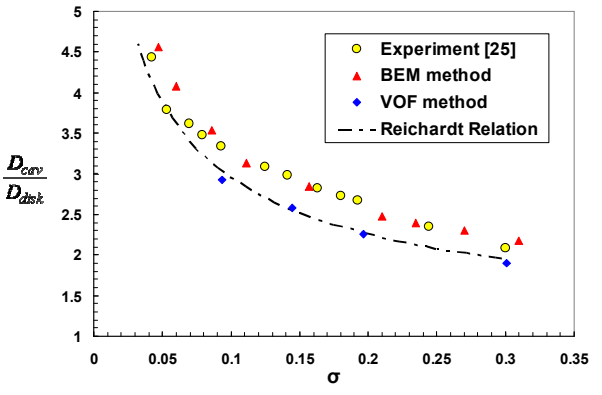

Fig. 4 Dimensionless cavity diameter vs. cavitation number for a disk cavitator.

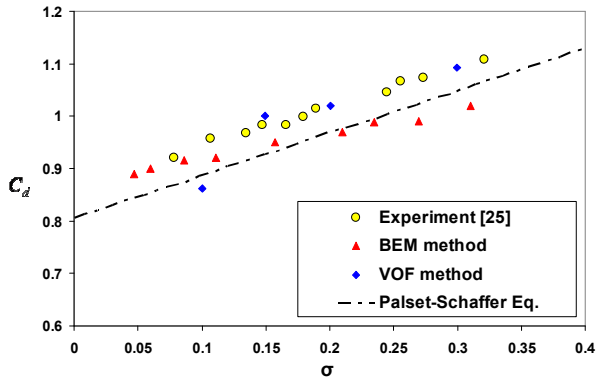

Fig. 5 Drag coefficient vs. cavitation number for a disk cavitator.

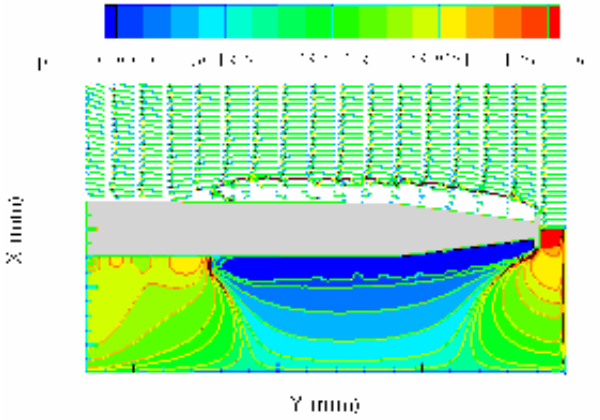

Fig. 6 The results of VOF model for a base case with R_c=0.25 and R_{cyl}= 0.9 for a cavitation number of σ = 0.0698. The image contains cavity shape, and velocity and pressure distributions. Pressures shown in this and all following figures are in Pascal.

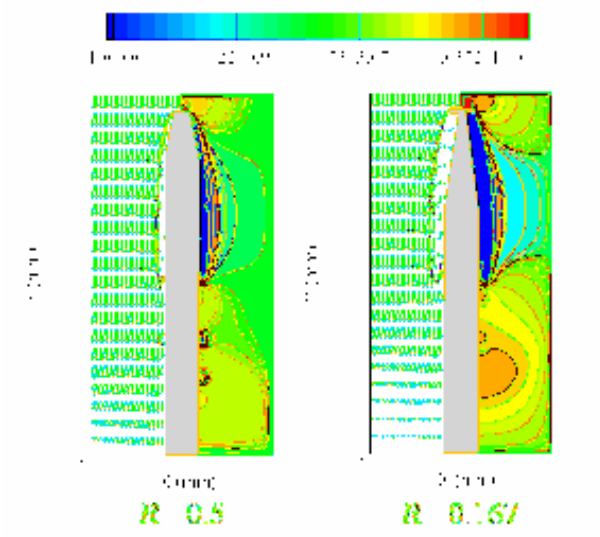

Fig. 7 The VOF method results for the effect of cone length (i.e. varying R_c at a constant R_{cyl} and cone angle) on the characteristics of cavitation for a cavitation number of 0.0698.

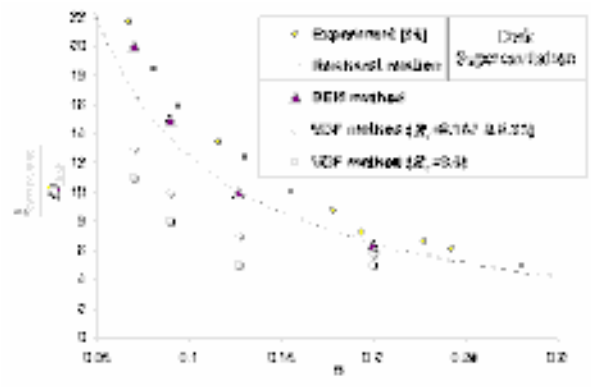

Fig. 8 Dimensionless cavity length vs. cavitation number for different cone length (by varying R_c). The results are shown using both VOF and BEM methods. The displayed experimental and analytical results should not be compared with those of the two methods (refer to the text in section 2.1).

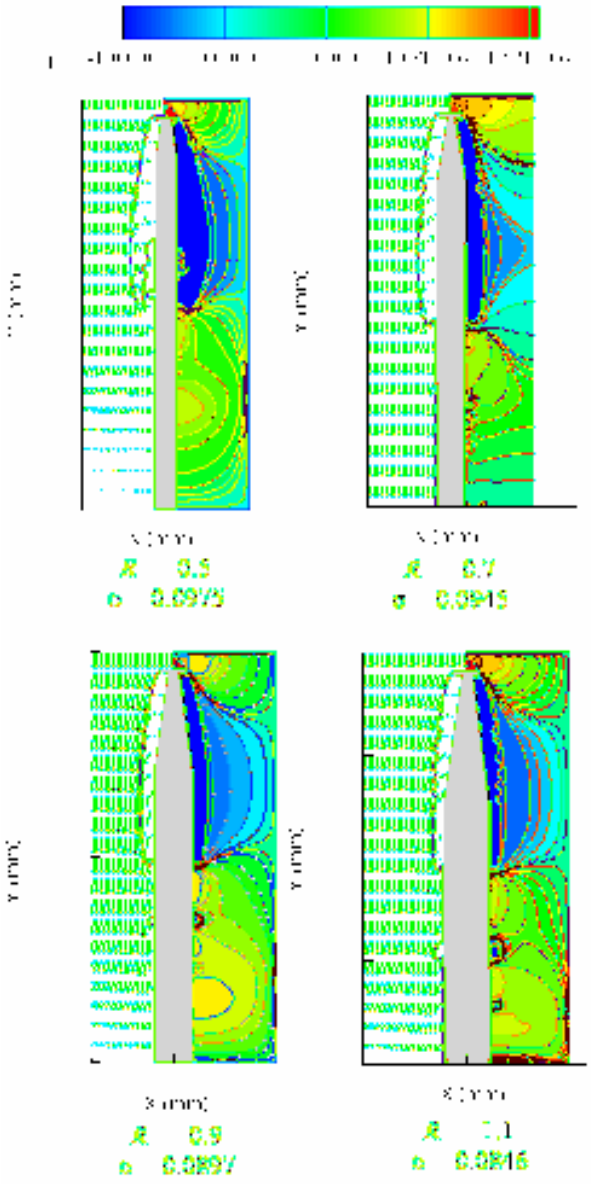

Fig. 9 The VOF method results for the effect of cylinder radius (at constant cone angle and R_c) on the characteristics of cavitation for a cavitation number of nearly 0.09.

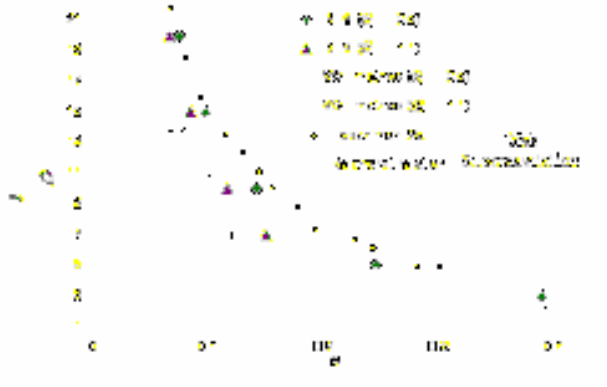

Fig. 10 Dimensionless cavitation length vs. cavitation number (R_{cyl}=0.5, 1.1). The displayed experimental and analytical results should not be compared with those of the two methods (refer to the text in section 2.1).

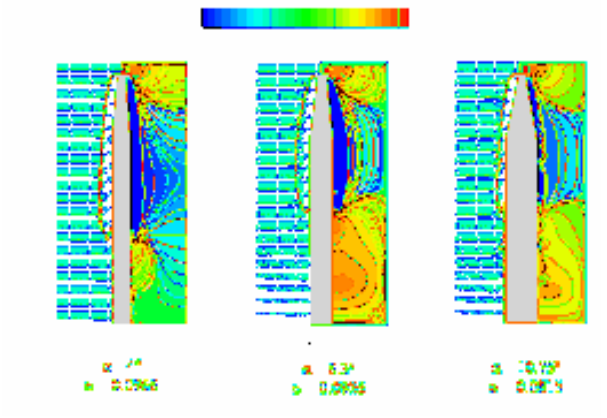

Fig. 11 The VOF method results for the effect of cone angle (at constant R_c) on the characteristics of cavitation for a cavitation number of nearly 0.09.

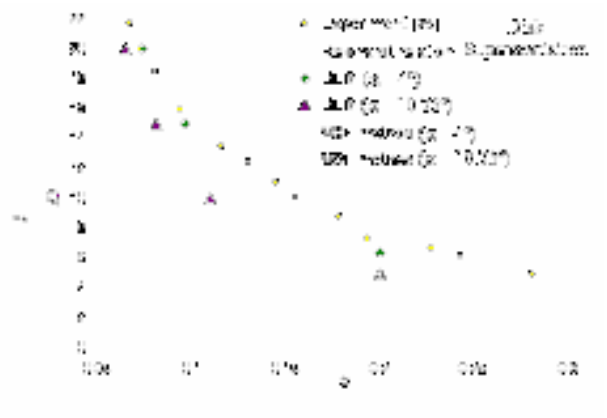

Fig. 12 Dimensionless cavitation length vs. cavitation number (α=4°, 6.3° , 10.75° or R_{cyl} = 0.6, 0.8, 1.2); R_c was held constant. The displayed experimental and analytical results should not be compared with those of the two methods (refer to the text in section 2.1).

References

1- M. Pasandideh-Fard and E. Roohi. "A Computational Model for Cavitation Using Volume-of-Fluid Method", In Proceedings of *the 3rd International Symposium on CFD Canada,* Kingston, Canada, 2006.

2- Abraham N. Varghese, James S. Ohlman and Ivan N. Kirschner. "High-speed bodies in partially cavitating axisymmetric flow", In proceedings of Fifth International Symposium on Cavitation (CAV2003), Osaka, Japan, Nov 2003

3- Xiaoxing Peng, Zhi Wang, Sensen Pan and Kai Yan. "Generation mechanism of ventilated supercavitation in an axisymmetric body with cavitator", In proceedings of Sixth International Symposium on Cavitation, CAV2006, Wageningen, The Netherlands, September 2006.

4- G. Wang, I. Senocak, W. Shyy, T. Ikohagi, and S. Cao, "Dynamics of attached turbulent cavitating flows" *Progress in Aerospace Sciences*, Vol. 37, pp. 551-581, 2001.

5- W. Yuan, J. Sauer and G.H. Schnerr, "Modeling and computation of unsteady cavitation flows in injection nozzles" *J. of Mechanical Ind.*, Vol. 2, pp. 383-394, 2001.

6- N. H. Singhal, A.K. Athavale, M. Li, and Y. Jiang, "Mathematical basis and validation of the full cavitation model" *J. of Fluids Engineering*, Vol. 124, pp. 1-8, 2002.

7- C.L. Merkle, J. Feng, and P.E.O. Buelow, "Computational modeling of the dynamics of sheet cavitation" in Proceedings of *the 3rd International Symposium on Cavitation, (CAV1998)*, Grenoble, France, 1998.

8- R.F. Kunz, D. A. Boger, D. R. Stinebring, T.S. Chyczewski, J.W. Lindau, and H. J. Gibeling, "A preconditioned Navier-Stokes method for two-phase flows with application to cavitation" *Computers & Fluids*, Vol. 29, pp. 849-875, 2000.

9- M. Frobenius and R. Schilling, Cav03-GS-9-005, "Three-dimensional unsteady cavitating effects on a single hydrofoil and in a radial pump- measurement and numerical simulation" in Proceedings of *the 5th International Symposium on Cavitation*, Osaka, 2003.

10- S. Wiesche, "Numerical simulation of cavitation effects behind obstacles and in an automotive fuel jet pump" *Heat Mass Transfer*, Vol. 41, pp. 615-624, 2005.

11- D.L. Youngs, "Time dependent multi material flow with large fluid distortion" *Num. Methods for Fluid Dynamics*, N.Y, 273-285, 1982.

12- J.L. Hess, A.M.O. Smith, "Calculation of potential flow about arbitrary three-dimensional bodies", Progress in Aeronautical Science,Vol. 8, pp. 1–138, Pergamon Press, New York, 1966.

13- J.S. Uhlman, "The Surface Singularity Method Applied to Partially Cavitating Hydrofoils," *J Ship Research,* 31, 2. 1987.

14- J.S. Uhlman, "The Surface Singularity or Boundary Integral Method Applied to Supercavitating Hydrofoils," *J Ship Research,* 33, 1. 1989.

15- S. A. Kinnas, and N.E. Fine, "Nonlinear Analysis of the Flow Around Partially and Super-Cavitating Hydrofoils by a Potential Based Panel Method," *Proceedings of the*

IABEM-90 Symposium, International Association for Boundary Element Methods, Rome, Italy, 1990.

16- S.A. Kinnas, and N.E. Fine, "A Numerical Nonlinear Analysis of the Flow Around Two- and Three-Dimensional Partially Cavitating Hydrofoils," *J Fluid Mech,* 254. 1993.

17- A.N. Varghese, J.S. Uhlman, and I.N. Kirschner "Axisymmetric Slender-Body Analysis of Supercavitating High-Speed Bodies in Subsonic Flow," *Proceedings of the Third International Symposium on Performance Enhancement for Marine Applications,* T. Gieseke, editor, Newport, RI, 1997.

18- I.N. Kirschner, J.S. Uhlman, Jr., A.N. Varghese, and I.M. Kuria, "Supercavitating Projectiles in Axisymmetric Subsonic Liquid Flows," *Proceedings of the ASME & JSME Fluids Engineering Annual Conference & Exhibition, Cavitation and Cavitation and Multiphase Flow Forum,* FED 210, J. Katz and Y. Matsumoto, editors, Hilton Head Island, SC, 1995.

19- J.S. Uhlman, A.N. Varghese, and I.N. Kirschner, "Boundary Element Modeling of Axisymmetric Supercavitating Bodies," *Proceedings of the 1st Symposium on Marine Applications of Computational Fluid Dynamics, Hydrodynamic/Hydroacoustic Technology Center,* McLean, VA, 1998.

20- Y.N. Savchenko, V.N. Semenenko, Y.I. Naumova, A.N. Varghese, J.S. Uhlman, and I.N. Kirschner "Hydrodynamic Characteristics of Polygonal Contours in Supercavitating Flow," *Proceedings of the Third International Symposium on Performance Enhancement for Marine Applications ,* T. Gieseke, editor, Newport, RI, 1997.

21- *Multiphase Flow Forum,* FED 210, J. Katz and Y. Matsumoto, editors, Hilton Head Island, SC.

22- F.H. Hirt and B.D. Nichols*,* "A computational method for free surface hydrodynamics" *J. Comput. Phys*., Vol. 39, p. 201, 1981.

23- J.U. Brackbill, D.B. Kothe and C. Zamach, "A continuum method for modeling surface tension, Comp. Physics" *J. Comput. Phys.*, Vol. 100, pp. 335-354, 1992.

24- I. Senocak and W. Shyy, "Evaluation of cavitation models for Navier-Stokes computations" Proceeding of FEDSM 02, ASME *Fluid Engineering Division Summer Meeting,* Montreal, Canada, 2002.

25- J.P. Franc and J.M. Michel*. "Fundamentals of Cavitation",* Section: 6. Kluwer Academic Publisher, Netherlands, 2004.R.E.